

Synchrotron Radiography Studies of Shear-Induced Dilation in Semisolid Al Alloys and Steels

C.M. GOURLAY,^{1,7} C. O'SULLIVAN,² J. FONSECA,³ L. YUAN,⁴
K.M. KAREH,¹ T. NAGIRA,⁵ and H. YASUDA⁶

1.—Department of Materials, Imperial College, London SW7 2AZ, UK. 2.—Department of Civil and Environmental Engineering, Imperial College, London SW7 2AZ, UK. 3.—Department of Civil Engineering, City University, London EC1V 0HB, UK. 4.—GE Global Research, Niskayuna, NY 12309, USA. 5.—Department of Adaptive Machine Systems, Osaka University, Suita, Osaka 565-0871, Japan. 6.—Department of Materials Science and Engineering, Kyoto University, Sakyo-ku, Kyoto 606-8501, Japan. 7.—e-mail: c.gourlay@imperial.ac.uk

An improved understanding of the response of solidifying microstructures to load is required to further minimize casting defects and optimize casting processes. This article overviews synchrotron radiography studies that directly measure the micromechanics of semisolid alloy deformation in a thin-sample direct-shear cell. It is shown that shear-induced dilation (also known as Reynolds' dilatancy) occurs in semisolid alloys with morphologies ranging from equiaxed-dendritic to globular, at solid fractions from the dendrite coherency point to ~90% solid, and it occurs in both Al alloys and carbon steels. Discrete-element method simulations that treat solidifying microstructures as granular materials are then used to explore the origins of dilatancy in semisolid alloys.

INTRODUCTION

Many casting defects have their origin in the natural flow, shrinkage/contraction and gas evolution that occurs during solidification. Additionally, it is common for a casting process to deform the solidifying alloy, either intentionally such as the application of pressure in high-pressure die casting and squeeze casting, or unintentionally such as the bulging between rolls in continuous casting. Therefore, to minimize casting defects and optimize casting processes, we require a detailed understanding of how solidifying microstructures respond to load and how deformation leads to casting defects.

Despite this importance, the study of semisolid alloy deformation has received little attention compared with fully solid alloys, and our understanding is much less developed. The focus of a large proportion of past work has been on either low-solid-fraction suspension rheology relevant to semisolid processing routes such as rheocasting,^{1–3} or on tensile loading at high solid fraction (>~0.90) relevant to hot tearing^{4–6}, and several combinations of semisolid microstructure and loading mode that remain largely unexplored.

A common mode of solidification in casting is the nucleation and growth of numerous equiaxed crystals. In the case that no other phase forms first, free crystals impinge on one another during growth, creating a crystal network.¹ This point is commonly termed “dendrite coherency,”^{7–9} although this term is also used to describe other transitions in the mushy zone.¹⁰ Dendrite coherency marks the onset of measurable shear and compressive strength, but the alloy has negligible tensile strength at this stage as there is negligible cohesion between crystals.^{1,11} Recently, it has been found that shear/compressive deformation at solid fractions above dendrite coherency causes shear-induced dilation¹² (also known as Reynolds' dilatancy¹³). This is the phenomenon in granular materials whereby the volume occupied by the particles/grains increases during shear (i.e., the packing density of the particles decreases during shear). This occurs when the particles are sufficiently densely packed that they push or lever one another apart as they begin to rearrange under load. Shear-induced dilation is a fundamental mechanical property of granular materials such as dense particulate soils¹⁴ and powders but was not expected of partially solid alloys.

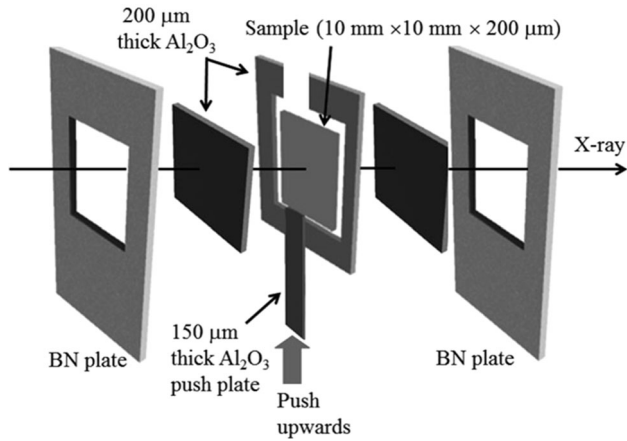


Fig. 1. Schematic of the thin-sample shear cell used for synchrotron radiography experiments on Al-Cu samples. N.B. samples were 180 μm thick in experiments on steels.

Subsequent studies have shown that dendrite coherency marks the onset of dilatancy (i.e., shear-induced dilation) in partially solid alloys,^{12,15,16} and it has been suggested that dilatancy may be important in semisolid processing,¹⁷ high-pressure die casting,¹⁸ and direct chill casting,¹⁹ for example, through dilatant shear banding. However, this remains a little explored area and the development of physically based models that include shear-induced dilation requires an improved understanding of the fundamentals. Therefore, the aims of this work have been: (I) to obtain direct proof of shear-induced dilation in semisolid alloys, (II) to understand the micromechanics of semisolid deformation at intermediate solid fractions and how this leads to shear-induced dilation, and (III) to explore modeling techniques that are well suited to capturing shear-induced dilation in semisolid alloys.

METHODS

Time-resolved synchrotron radiography experiments were performed in a thin-sample direct-shear cell shown in Fig. 1, which is loosely based on the direct shear-box test in soil mechanics (e.g., Ref. 20). The rig was developed to study assemblies of numerous equiaxed crystals that are approximately one crystal thick. All semisolid deformation experiments were conducted isothermally on partially remelted samples. A variety of semisolid grain morphologies were created by altering the prior solidification and coarsening treatments. For example, an equiaxed-dendritic morphology was generated by partially remelting an equiaxed-dendritic cast microstructure and isothermally holding for 20 min prior to deformation. Globular morphologies were generated by applying a ~ 1 week semisolid heat treatment prior to partial remelting, thermal equilibration, and deformation. All experiments reported here involved combinations of solid fraction and crystal morphology that

resulted in an assembly of crystals in mechanical contact.

The rig was incorporated into beamline BL20B2 at the SPring-8 synchrotron in Hyogo, Japan.²¹ As depicted in Fig. 1, the pushing plate penetrates vertically upward and the displacement rate was set to $du_z/dt = 100 \mu\text{m s}^{-1}$, giving a global shear rate of $\sim 1 \times 10^{-2} \text{ s}^{-1}$. Deformation was conducted to accumulated global shear strains of $\gamma \sim 10\text{--}30\%$. Some experiments were conducted on Al-15Cu alloys, which have strong solid-liquid contrast in the transmitted x-ray images. Other experiments were conducted on Fe-2C alloys to develop the deformation/imaging technique toward industrially relevant steels. In carbon steels, the γ -Fe and liquid phases have only weak x-ray absorption contrast, and the imaging challenges have only recently been overcome as overviewed in Ref. 22. Full experimental details on imaging and deformation can be found in Ref. 23 for Al-Cu alloys and Ref. 24 for Fe-C alloys.

RESULTS AND DISCUSSION

General Phenomena

The phenomenon of shear-induced dilation is summarized in Fig. 2a and b for the simplified case of ordered packings of circles in homogeneous compressive loading modes. The figure depicts quasi-rigid grains with negligible intergrain cohesion where force is transmitted across grain-grain contacts and the resulting macroscopic shape change occurs by grain rearrangement. This behavior is often termed granular deformation, and the materials that exhibit this behavior are often termed packed granular materials.²⁵ It can be seen that, under these conditions, geometry dictates that the application of a shear strain generates volumetric strain, accommodated by an increase in the volume of interstitial spaces. Note that strain is defined here with respect to the solid assembly, so that a decreasing packing density of the grains is defined as a dilatational volumetric strain.¹⁴ For the case of homogeneous shear of uniform circles from the close packed to least packed configuration (from a hexagonal array to square array), the volumetric strain is a $\sim 15.5\%$ dilation ($\frac{2}{\sqrt{3}} - 1$). Note that the continued shear of Fig. 2b would lead to the grains being pushed closer together again (a contractive volumetric strain), and to cyclic dilation and contraction. This is a feature of the ordered packing of monodisperse circles. In disordered polydisperse packings found in nature (e.g., soils, powders, etc.), there are local regions of compaction and dilation, and the overall volumetric strain comes from a combination of local dilation and compaction that is either net-contractive, net-dilatational, or constant-volume deformation.

It might be thought that partially solid alloys containing a solid network would not deform in this way because the grains have a yield strength of only

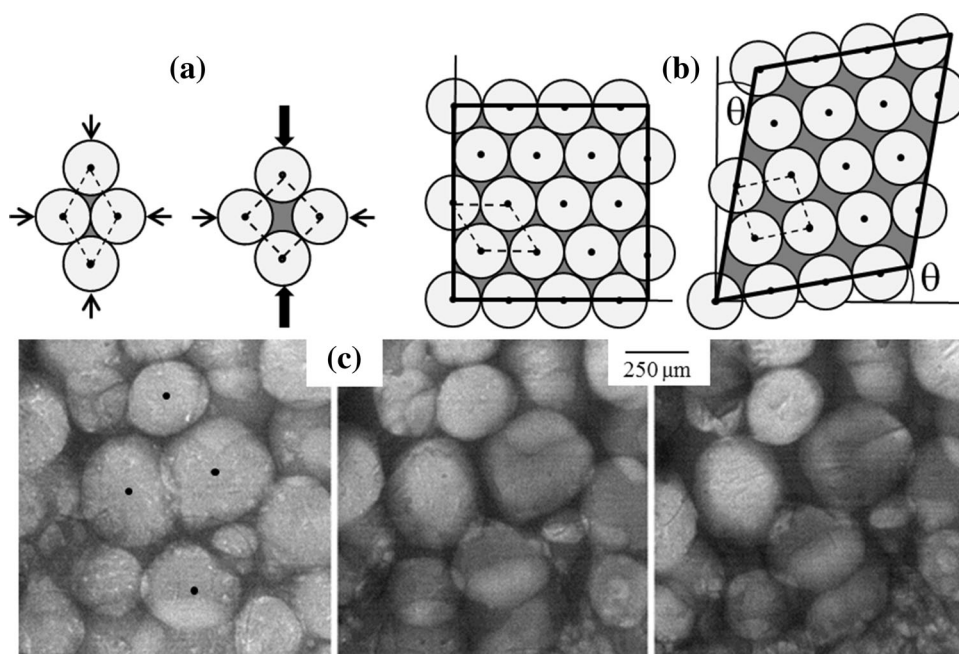


Fig. 2. (a, b) Shear-induced dilation of ordered close-packed circles: (a) four circles in biaxial compression and (b) 20 circles in pure shear. Grains are light gray, grain centroids are marked with dots, interstitial liquid is shaded dark grey and arrows indicate the direction and magnitude of force. (c) Four globules in Al-15Cu at $\sim 70\%$ solid (centroids marked with dots) loaded similar to (a).

up to a few MPa at $T/T_m \sim 1$,^{1,26,27} and grain–grain contacts can be cohesive due to the formation of solid–solid interfaces (grain boundaries) where the misorientation angle is favorable.^{28,29} However, direct *in situ* imaging has shown that semisolid alloys often deform by shear-induced dilation.^{23,24,30,31} As an example, Fig. 2c shows a local region of microstructure where the configuration of four grains and the loading direction are similar to the geometry in Fig. 2a. In Fig. 2c, it can be directly observed that, during loading, the grains push each other apart in a manner similar to Fig. 2a. It can also be seen that the expansion of interstitial spaces is compensated by the inflow of liquid (dark) from elsewhere in the sample. The absence of observed cohesion between grains suggests that the relationship of $\sigma_{S-S} > 2\sigma_{S-L}$ is generally satisfied for most grain–grain misorientations (σ = interfacial energy) and that liquid films exist between grains.

In general, partially solid alloy microstructures that develop during equiaxed solidification are disordered packings of polydisperse grains with complex shapes and complex contacts. Therefore, *in situ* studies were performed on semisolid alloys of a variety of solid fractions and crystal morphologies to study the micromechanics in a range of semisolid alloys.^{23,24,31} These studies have found that, during loading in the shear cell, the microstructural response to load shares common features whenever the partially solid alloy consists of numerous grains in mechanical contact and there is sufficient interstitial liquid to feed volumetric strains. These common features are as follows:

1. There is rarely any discernible deformation of the individual grains (see the section, “Equiaxed-Dendritic Al-15Cu at $\sim 30\%$ Solid” for an exception to this statement).
2. Macroscopic deformation occurs predominantly by grain rearrangement coupled with interstitial liquid flow.
3. Most grains translate and rotate as discrete bodies under the action of contact forces.
4. After loading, there is an adjustment of grain positions that causes changes in the local grain-packing density (the local solid fraction) so that the overall response comes from a combination of local dilation and local compaction. For the combinations of solid fraction, morphology, and strain rate overviewed in this article, changes in solid fraction were accommodated by the inflow or outflow of the interstitial liquid from other regions of the samples. An analysis of the grains has confirmed that there was no measurable remelting or solidification during testing in the experiments in this article.
5. Macroscopic shear-induced dilation occurs causing the overall solid fraction to decrease during grain rearrangement.
6. Grain motion often becomes localized in certain areas, producing inhomogeneous deformation.

We next focus on the detailed grain-scale response to load in three data sets from microstructures containing numerous equiaxed grains in mechanical contact but that have markedly different semisolid microstructures: equiaxed-dendritic at $\sim 30\%$ solid,

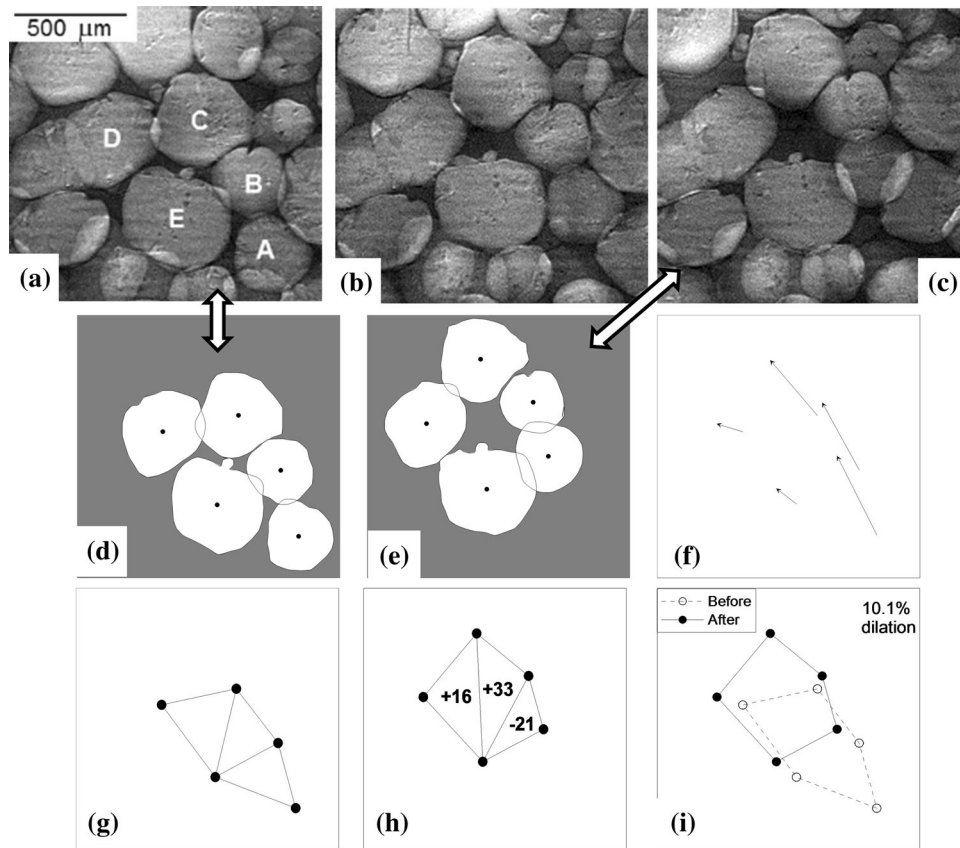


Fig. 3. Local region of shear-induced dilation in globular Al-15Cu. (a–c): Radiographs of globules pushing each other apart during rearrangement. (d and e): Projected-area globule outlines and centroids. (f) Centroid displacements from (d) to (e). (g and h): Triangulation of the globule centroids. The values in (h) are the % volumetric strain of the triangles. (i) Overall area change of the centroid polygons = 10.1% dilation.

globular at $\sim 70\%$ solid, and globular-polygonal at $\sim 88\%$ solid.

Globular Al-15Cu at $\sim 70\%$ Solid

Figures 3 and 4 overview results from a globular Al-15Cu sample deformed at $\sim 70\%$ solid (produced by an 8-day semisolid heat treatment to globularize the α Al prior to the experiment). It can be seen that the initial microstructure is a disordered assembly of grains in mechanical contact with liquid filling the interstitial spaces. The sample thickness is ~ 0.6 median grain diameters, producing a near-monolayer of grains that have been sectioned into “disks” during sample preparation, and there is some overlap between the grains in the projected-area images. During loading in the shear cell, there are regions of local compaction and local dilation.

An example of local dilation is overviewed in Fig. 3, which is a region near the half-plane of the shear cell. Note that the pushing plate is located at the bottom right of the grain labeled A in Fig. 3a. As the plate moves upward, grain A pushes B and C up and to the left, and A, B, and C slide past D and E between Fig. 3a and b. Now A is in contact with both B and E and, as A is pushed further up and to the left, the position of the contacts between A–B

and A–E causes grain A to push B and E apart (compare Fig. 3b and c). These grain movements are due to force transmission across contacts and cause the packing density of the grains to decrease and the volume of the liquid-filled intergrain spaces to increase. The projected grain perimeters and centroids corresponding to Fig. 3a and c are plotted in Fig. 3d and e, respectively. The centroid displacement field (Fig. 3f) contains diverging vectors because the grains are pushing each other apart. In Fig. 3g–i, the local dilatational volumetric strain is quantified by triangulation of the centroids in Fig. 3d and e. The values in each triangle show the volumetric strain in each triangle, and the overall dilation of this local assembly is 10.1% as shown in Fig. 3i.

Figure 4 is the same region as that in Fig. 3 but spans a longer period of deformation. In Fig. 4, it can be inferred from the motion of grain C that this grain is actually welded to (has a grain boundary with) the smaller grain to its right, making an effective structural unit (an agglomerate) shaped like a bowling pin. In Fig. 3, grain C only translates upward, but in Fig. 4 grain C undergoes significant rotation. This can be understood by considering the position of the two contacts marked with white dots in Fig. 4 and noting that the contact normal force is

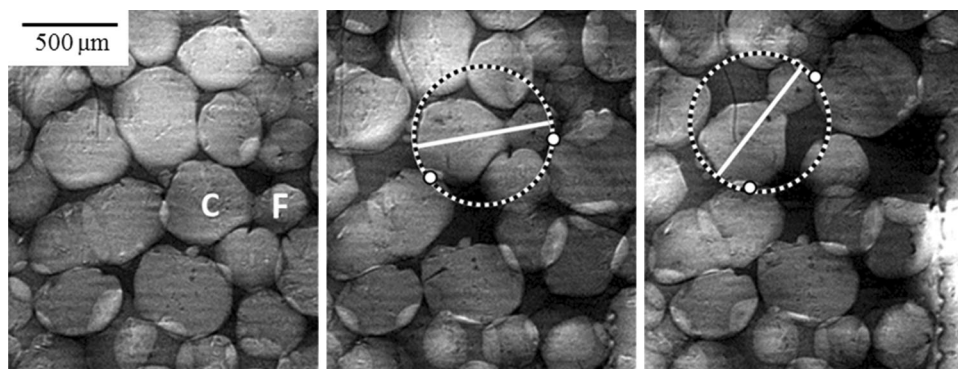


Fig. 4. Deformation of globular Al-15Cu at $\sim 70\%$ solid, highlighting the role of the rotation of an agglomerate of grains C and F with bowling pin shape. White dots mark the contacts important in causing rotation, white lines are the primary axis of the agglomerate formed by grains C and F, and the dashed line is the circle with diameter equal to the primary axis of the agglomerate. The push plate can be seen to the far right of each image.

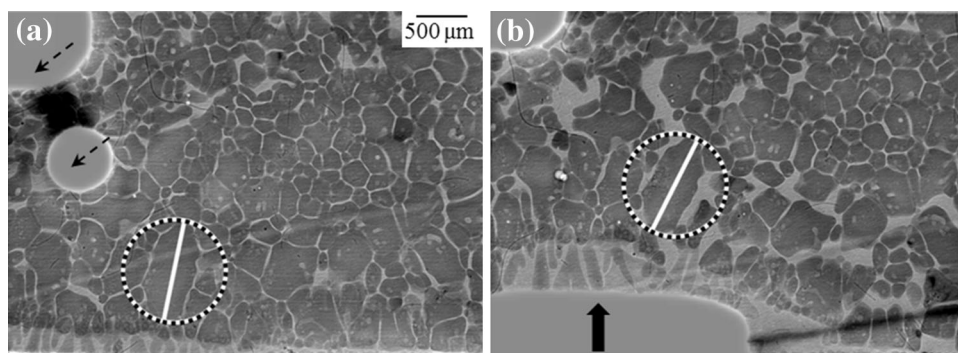


Fig. 5. Deformation of globular-polygonal Fe-2C-1Mn-0.5Si at $\sim 88\%$ solid: (a) prior to deformation and (b) after 1072 μm (3.1 mean grains) of push-plate displacement. Note the significantly enlarged liquid-filled interstices in (b) due to shear-induced dilation. The primary axis and circle of rotation are shown for a large grain with high aspect ratio. Austenite is dark gray, liquid is light gray, and the rounded features marked with arrows are pores.

not collinear with the vector joining the centroids (the branch vector), causing the contact normal force to apply a significant moment. Between Fig. 4b and c, the major axis of the bowling pin agglomerate undergoes a 46° anticlockwise rotation, which creates significant interstitial space because the bowling pin shape sweeps out a much larger projected area than its true projected area. Therefore, the rotation of grain C with high aspect ratio causes strong local dilation.

Globular-Polygonal Fe-2C-1Mn-0.5Si at $\sim 88\%$ Solid

Figure 5 shows images of the entire field of view at two stages during the deformation of a semisolid high-carbon steel at $\sim 88\%$ solid. This sample was produced by an extended semisolid heat treatment of 100 h at $\sim 70\%$ solid under Ar.³¹ The combination of the high solid fraction and semisolid coarsening treatment has created a grain morphology that is partially globular and partially polygonal, with some solid-liquid interfaces that are concave to accommodate the convex solid-liquid interfaces of

neighboring grains and with many interfaces that are relatively straight. Note that austenite grains are dark and the liquid bright in Fig. 5 (the opposite of the Al-Cu radiographs).

It can be seen in Fig. 5 that deformation at such high solid fraction leads to strong shear-induced dilation with large liquid-filled spaces opening up between grains during shear. As discussed in Ref. 31, this liquid was drawn in from the sides of this sample, and there was no measurable deformation of the individual grains at the resolution of the experiment.

Similar to the globular sample at $\sim 70\%$ solid in Figs. 3 and 4, shear-induced dilation in Fig. 5 is caused by the translation and rotation of quasi-rigid grains that were initially tightly packed. The rotation of a large grain with a relatively high aspect ratio is highlighted in Fig. 5. This grain rotates 14° clockwise between the two frames in Fig. 5, which levers neighboring grains apart and creates significant interstitial space.

The inhomogeneous strain field can be quantified from these experiments by first segmenting the grains and triangulating the grain centroids. Then,

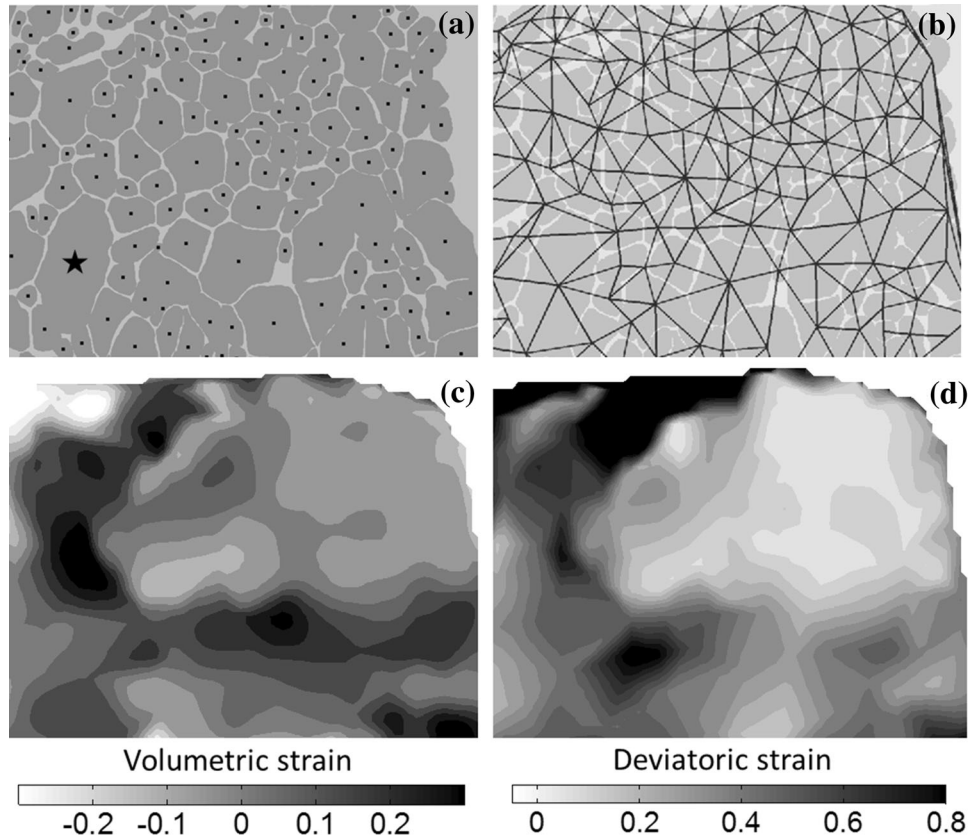


Fig. 6. (a) Separated grains and their centroids from part of Fig. 5a. The centroid marked with a star is the grain highlighted in Fig. 5. (b) Delaunay triangulation of the centroids. (c) Volumetric strain field where positive values indicate dilation. (d) Deviatoric strain field. The strain fields have been smoothed and are for the deformation increment from Fig. 5a and b.

the strain in each triangle, defined by a triad of three centroids, can be calculated from the centroid displacements using the constant strain triangle shape functions from finite-element analysis (e.g., Ref. 32) in a way similar to Fig. 3h. This has been performed for a portion of the steel data set from Fig. 5, and the results are shown in Fig. 6. Figure 6a is a plot of the segmented and separated grains, and their centroids in the undeformed state. Figure 6b is a Delaunay triangulation of the initial centroids, and Fig. 6c and d are the volumetric and deviatoric strain fields, respectively, for the deformation increment shown in Fig. 5. The strain fields have been smoothed to aid visualization because there are large variations in strain from triangle to triangle (as can be seen for volumetric strain in Fig. 3h). Note that there are local regions of positive and negative volumetric strain, and the overall behavior is net-dilatational. In Fig. 6d, the shear strains are taken as the difference between the eigenvalues of the strain tensor in each triangle.

Figure 6c and d quantify the inhomogeneous volumetric and shear strain fields. It can be seen that, in general, regions of high shear correspond to regions of high dilation. A region of high shear and simultaneous dilation has developed both in a vertical band and a horizontal band that start close to

the large grain highlighted in Fig. 5. As shown in Ref. 31, the regions of high shear and dilatational volumetric strain in this sample correspond to regions of highest grain rotation, the greatest reduction in number of contacts per grain, and the greatest increase in distance between neighboring grains.

Equiaxed-Dendritic Al-15Cu at ~30% Solid

Since macroscopic rheology experiments have measured that the dendrite coherency point marks the onset of dilatancy in equiaxed solidification,^{12,15,16} *in situ* experiments were conducted on equiaxed-dendritic microstructures slightly above the dendrite coherency point. Figure 7a shows Al-15Cu at ~30% solid with an equiaxed-dendritic morphology, produced by partially remelting a coarse equiaxed-dendritic cast microstructure and isothermally holding for 20 min prior to deformation.²³ This combination of crystal morphology and low solid fraction results in an assembly of crystals in contact because a significant proportion of the liquid is within dendrite envelopes and the envelopes are in mechanical contact. Note that for equiaxed solidification in general, although the dendrite coherency solid fraction can vary from

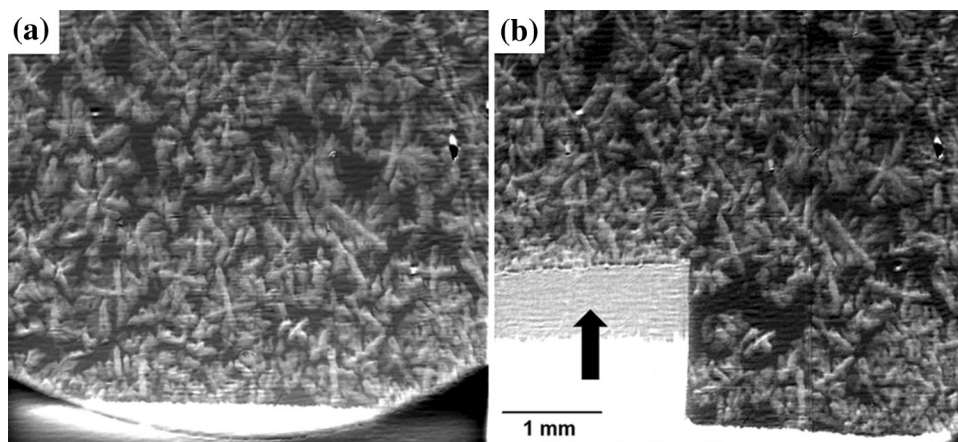


Fig. 7. Radiographs of Al-15Cu with equiaxed-dendritic morphology at $\sim 30\%$ solid: (a) prior to deformation and (b) after $1606\ \mu\text{m}$ (3.8 mean grains) of push-plate displacement.

~ 0.15 to 0.5 ^{7,8} the envelope fraction at coherency has been shown to fall within a much higher and narrower range of 0.56 – 0.70 ³³ (note, a dendrite envelope is defined here as the volume bounded by the surface connecting the primary and secondary arm tips of a dendrite).

Comparing Fig. 7a and b, it can be seen that in most of the field of view, deformation was accommodated by grain rearrangement by discrete translations and rotations of the crystal envelopes. The exception to this occurred at the pushing-plate front where global deformation occurred by crystal deformation, and the crystal assembly deformed as a viscoplastic solid skeleton that squeezed out interstitial liquid as it was compressed. This shows that there is added complexity in equiaxed-dendritic structures caused by a competition between deformation of the individual grains and rearrangement of grains that was not measured for the globular and globular-polygonal structures in sections titled, “Globular Al-15Cu at $\sim 70\%$ Solid” and “Globular-Polygonal Fe-2C-1Mn-0.5Si at $\sim 88\%$ Solid.”

Away from the small region at the leading edge of the pushing plate where the individual grains were deformed, shape change occurred by rearrangement of the envelopes. Dendritic grain rearrangement caused local compaction and local dilation. An example of local dilation is shown in Fig. 8 involving 12 crystals labeled A–L. In Fig. 8a and b, the liquid-filled space between the 12 envelopes dilates because the dendritic grains push and lever each other apart similar to the globular grains in Fig. 3. Note that the pushing-plate displacement between Fig. 8a and b is $\sim 0.2 d_{50}$ (where d_{50} is the median projected grain size). Of particular importance in this dilation event is the small clockwise rotation of grain G, which pushes grain H upward and grain I down and to the right, creating interstitial space. The projected grain perimeters and centroids corresponding to Fig. 8a and b are plotted in Fig. 8c and d, respectively. The centroid displacement field

in Fig. 8e shows that the grains are moving to the right, away from the advancing pushing plate, and that there is a slight divergence to the vectors. In Fig. 8f and g, the local dilatational volumetric strain is quantified by triangulation of the centroids in Fig. 8c and d. The values in each triangle show the volumetric strain in each triangle, and the overall dilation of this local assembly is 1.9% as shown in Fig. 8h.

Comparing the deformation of the equiaxed-dendritic microstructure in Figs. 7 and 8 with the globular microstructure in Figs. 3 and 4 and the globular-polygonal microstructure in Figs. 5 and 6, there are a variety of differences in the details of the micromechanics. For example, the contacts across which force is transmitted in the equiaxed-dendritic and globular microstructures are relatively well approximated as point contacts similar to the circles in Fig. 2a and b. In contrast, a high proportion of each grain perimeter is involved in force transmission in the globular-polygonal microstructure in Figs. 5 and 6. Additionally, the magnitude of the shear-induced dilation is significantly different in each microstructure, which is mostly because of the different initial packing-densities of the crystal envelopes. Despite these differences, each microstructure deforms predominantly by grain rearrangement and undergoes shear-induced dilation, highlighting the ubiquity of this phenomenon in equiaxed semisolid microstructures containing a solid network.

Discrete-Element Method (DEM) Modeling

During experiments on semisolid alloys containing a solid network, the synchrotron radiography studies have shown that shape change predominantly occurs by the rearrangement of grains within an assembly of grains in mechanical contact and that shear-induced dilation is a fundamental part of the microstructural response to load. Other materials that exhibit these deformation phenomena

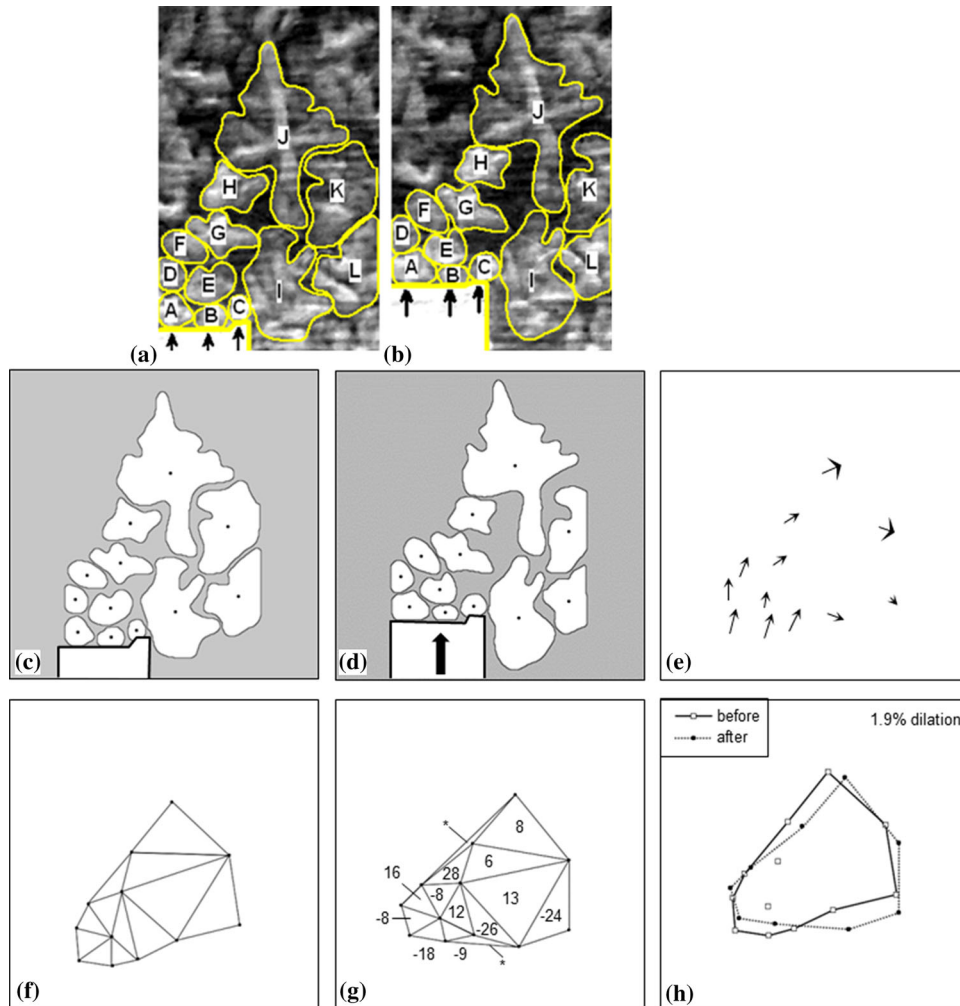


Fig. 8. Local region of shear-induced dilation in equiaxed-dendritic Al-15Cu at $\sim 30\%$ solid. (a, b): Radiographs of 12 crystals with envelopes estimated in yellow. (c and d): Projected-area envelope outlines and centroids. (e) Centroid displacements from (c) to (d). (f and g): Triangulation of the globule centroids. The values in (g) are the % volumetric strain of the triangles. (h) Overall area change of the centroid polygons = 1.9% dilation.

such as soils,³⁴ powders, and other compacted granular materials are often modeled using the particulate DEM. In DEM, the material is explicitly treated as an assembly of rigid particles that can move independently by translation and rotation caused by forces acting at particle–particle contacts,³⁵ and shear-induced dilation emerges naturally with this approach.

A DEM model was developed within the commercial DEM package PFC^{2D} (Itasca Consulting Group, Inc. based on Ref. 35) that takes simulated two-dimensional (2D) solidification microstructures as inputs and models the microstructural response to an imposed deformation.³³ The study in Ref. 33 used equiaxed solidification microstructures modeled with the approach from Lee and co-workers.³⁶ We showed that dendrite coherency can be considered to be the lowest solid fraction at which long-range interconnectivity in the force chain network develops during shear, and we confirmed that dendrite coherency marks the lowest solid fraction at

which shear-induced dilation occurs. The study can also be used to gain insights on shear-induced dilation in a grain assembly created by equiaxed solidification.

Figure 9 shows a simulated 2D equiaxed-dendritic microstructure that was deduced to be above the dendrite coherency solid fraction in Ref. 33. The figure shows a DEM simulation of this microstructure during loading in direct-shear with some similarities to the thin-sample shear cell in Fig. 1. In this DEM simulation, the left-hand side wall is defined as stationary and a constant stress condition has been applied to the right-hand side wall such that if the stress acting on the right-hand wall reaches a critical value, then the right-hand wall adjusts its horizontal displacement and a constant stress is maintained by a servo-mechanism. Full details are given in Ref. 33. White lines are drawn between the centroids of contacting particles and the line thickness is proportional to force magnitude. It can be seen that as the pushing-plate begins

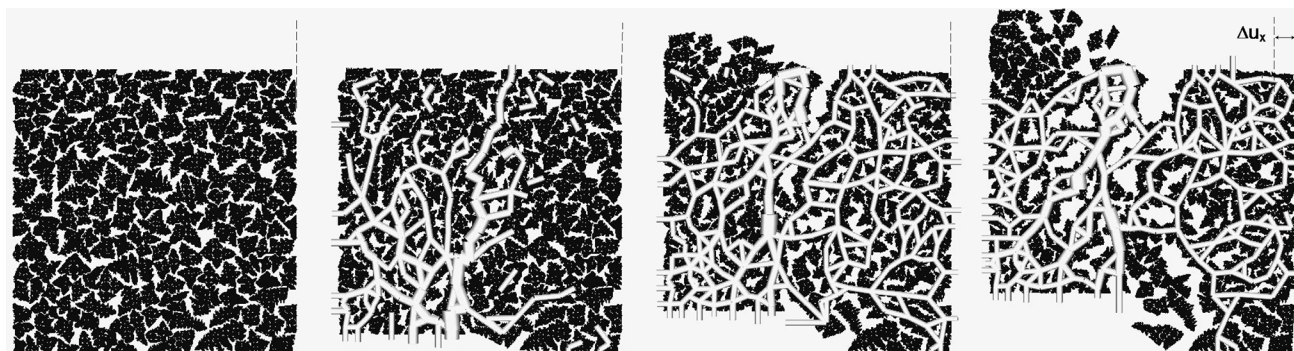


Fig. 9. Two-dimensional DEM simulation of shear-induced dilation in an equiaxed-dendritic microstructure deformed in direct shear. The left-hand side wall is stationary and a constant stress condition has been applied to the right-hand side wall such that it adjusts its horizontal displacement to maintain a constant stress. Dashed black lines are the initial right-hand wall position and solid black lines are the current position. The white lines are force chains with line thickness proportional to force magnitude. Force is transmitted across crystal–crystal contacts and shear-induced dilation Δu_z emerges naturally from the simulation. Full details are given in Ref. 33.

to move upward, grain–grain contacts are created through which force can be transmitted and a so-called network of force chains develops vertically. With continued pushing-plate displacement, the force chain network develops throughout most of the sample and force is transmitted to the right-hand side wall. With further pushing-plate displacement, there comes a point when the critical stress on the right-hand wall is exceeded and the right-hand wall moves to the right, leading to a dilatational volumetric strain. This can be seen by noting that dashed black lines are the initial right-hand wall position and solid black lines are the current position. In this way, shear-induced dilation emerges naturally from the simulation. It is also of interest to note that if the crystal assembly is constrained to rearrange at constant volume and the grains are defined to be rigid, then this microstructure becomes jammed (as shown in Fig. 4c, f, and i in Ref. 33). Thus, we would expect the mechanical response to be pressure sensitive and the competition between grain rearrangement and the deformation of individual grains to be pressure sensitive.

Particulate numerical modeling including the DEM has been applied to semisolid alloy deformation by other groups,^{37–39} which are combining finite-element and discrete-element methods to account for the viscoplastic deformation of the solid. The *in situ* imaging results and these initial models suggest that DEM is likely to be an important component within future models of metallic alloy mush mechanics.

SUMMARY

In situ studies of semisolid deformation have provided direct proof for shear-induced dilation in semisolid alloys with morphologies ranging from equiaxed-dendritic to globular and solid fractions ranging from dendrite coherency to $\sim 90\%$ solid. It has been shown that this behavior is the result of

load transmission across grain–grain contacts and grains rearranging as largely cohesionless, quasi-rigid bodies within a network of grains in mechanical contact. It has been shown that these deformation characteristics can be captured by the DEM, which has significant potential as a component of mush mechanics models.

ACKNOWLEDGEMENTS

Experiments were conducted at the SPring-8 synchrotron on beamline BL20B2 under proposal numbers 2008A-1428 and 2011A-1209 and were supported by a Grant-in-Aid for Scientific Research (S), MEXT, Japan. The analysis was carried out under grant EP/K026763/1 (EPSRC) and with a Royal Society Daiwa Anglo-Japanese Foundation International Exchanges Award.

REFERENCES

1. M.C. Flemings, *Metall. Trans. A* 22, 957 (1991).
2. H.V. Atkinson, *Prog. Mater. Sci.* 50, 341 (2005).
3. S. Zabler, A. Ershov, A. Rack, F. Garcia-Moreno, T. Baumbach, and J. Banhart, *Acta Mater.* 61, 1244 (2013).
4. M. M'Hamdi, A. Mo, and C.L. Martin, *Metall. Mater. Trans. A* 33, 2081 (2002).
5. S. Terzi et al., *Scr. Mater.* 61, 449 (2009).
6. D.G. Eskin, Suyitno, and L. Katgerman, *Prog. Mater. Sci.* 49, 629 (2004).
7. L. Arnberg, G. Chai, and L. Bäckerud, *Mater. Sci. Eng. A* 173, 101 (1993).
8. N.L.M. Veldman, A.K. Dahle, D.H. StJohn, and L. Arnberg, *Metall. Mater. Trans. A* 32A, 147 (2001).
9. A.K. Dahle and L. Arnberg, *Acta Mater.* 45, 547 (1997).
10. J.A. Dantzig and M. Rappaz, *Solidification* (Lausanne: EPFL Press, 2009).
11. A.K. Dahle, S. Instone, and T. Sumitomo, *Metall. Mater. Trans. A* 34, 105 (2003).
12. C.M. Gourlay and A.K. Dahle, *Nature* 445, 70 (2007).
13. O. Reynolds, *Philos. Mag.* 20, 469 (1885).
14. A. Schofield and C. Wroth, *Critical State Soil Mechanics* (Columbus, OH: McGraw-Hill, 1968).
15. C.M. Gourlay, B. Meylan, and A.K. Dahle, *Acta Mater.* 56, 3403 (2008).
16. B. Meylan, S. Terzi, C.M. Gourlay, and A.K. Dahle, *Acta Mater.* 59, 3091 (2011).
17. F. Pineau and G. Simard, *Solid State Phenom.* 141, 635 (2008).

18. C.M. Gourlay, H.I. Laukli, and A.K. Dahle, *Metall. Mater. Trans. A* 38, 1833 (2007).
19. T. Carlberg and A.E.W. Jarfors, *Metall. Mater. Trans. B* 45, 175 (2014).
20. W. Powrie, *Soil Mechanics: Concepts and Applications*, 2nd ed. (Oxford: Spon Press, 2002).
21. S. Goto, K. Takeshita, Y. Suzuki, H. Ohashi, Y. Asano, and H. Kimura, *Nucl. Instrum. Methods A* 467, 682 (2001).
22. H. Yasuda, T. Nagira, M. Yoshiya, N. Nakatsuka, A. Sugiyama, K. Uesugi, and K. Umetani, *ISIJ Int.* 51, 402 (2011).
23. C.M. Gourlay, A.K. Dahle, T. Nagira, N. Nakatsuka, K. Nogita, K. Uesugi, and H. Yasuda, *Acta Mater.* 59, 4933 (2011).
24. T. Nagira, C.M. Gourlay, A. Sugiyama, M. Uesugi, Y. Kanzawa, M. Yoshiya, K. Uesugi, K. Umetani, and H. Yasuda, *Scr. Mater.* 64, 1129 (2011).
25. H.M. Jaeger and S.R. Nagel, *Science* 255, 1523 (1992).
26. J. Pilling and A. Hellawell, *Metall. Mater. Trans. A* 27A, 229 (1996).
27. D. Fuloria and P.D. Lee, *Acta Mater.* 57, 5554 (2009).
28. M. Rappaz, A. Jacot, and W.J. Boettinger, *Metall. Mater. Trans. A* 34, 467 (2003).
29. O. Ludwig, J.M. Drezet, C.L. Martin, and M. Suéry, *Metall. Mater. Trans. A* 36A, 1525 (2005).
30. T. Nagira, H. Yokota, S. Morita, H. Yasuda, M. Yoshiya, C.M. Gourlay, A. Sugiyama, K. Uesugi, and K. Umetani, *ISIJ Int.* 53, 1195 (2013).
31. J. Fonseca, C. O'Sullivan, T. Nagira, H. Yasuda, and C.M. Gourlay, *Acta Mater.* 61, 4169 (2013).
32. C. O'Sullivan, J.D. Bray, and S.F. Li, *Int. J. Numer. Anal. Metall.* 27, 859 (2003).
33. L. Yuan, C. O'Sullivan, and C.M. Gourlay, *Acta Mater.* 60, 1334 (2012).
34. C. O'Sullivan, *Particulate Discrete Element Modelling: A Geomechanics Perspective* (Florence, KY: Taylor & Francis, 2011).
35. P.A. Cundall and O.D.L. Strack, *Geotechnique* 29, 47 (1979).
36. W. Wang, P.D. Lee, and M. McLean, *Acta Mater.* 51, 2971 (2003).
37. S. Vernède, P. Jarry, and M. Rappaz, *Acta Mater.* 54, 4023 (2006).
38. M. Sistaninia, A.B. Phillion, J.M. Drezet, and M. Rappaz, *Metall. Mater. Trans. A* 42A, 239 (2011).
39. A.B. Phillion, S. Vernède, M. Rappaz, S.L. Cockcroft, and P.D. Lee, *Int. J. Cast Met. Res.* 22, 240 (2009).